

Present status and future challenges of non-interferometric tests of collapse models

Matteo Carlesso¹, Sandro Donadi², Luca Ferialdi^{2,3}, Mauro Paternostro¹, Hendrik Ulbricht⁴, and Angelo Bassi^{2,3,*}

¹Centre for Theoretical Atomic, Molecular, and Optical Physics, School of Mathematics and Physics, Queens University, Belfast BT7 1NN, United Kingdom

²Istituto Nazionale di Fisica Nucleare, Trieste Section, Via Valerio 2, 34127 Trieste, Italy

³Department of Physics, University of Trieste, Strada Costiera 11, 34151 Trieste, Italy

⁴School of Physics and Astronomy, University of Southampton, SO17 1BJ Southampton, United Kingdom

*abassi@units.it

ABSTRACT

The superposition principle is the cornerstone of quantum mechanics, leading to a variety of genuinely quantum effects. Whether the principle applies also to macroscopic systems or, instead, there is a progressive breakdown when moving to larger scales, is a fundamental and still open question. Spontaneous wavefunction collapse models predict the latter option, thus questioning the universality of quantum mechanics. Technological advances allow to challenge collapse models and the quantum superposition principle more and more with a variety of different experiments. Among them, non-interferometric experiments proved to be the most effective in testing these models. We provide an overview of such experiments, including cold atoms, optomechanical systems, X-rays detection, bulk heating as well as comparisons with cosmological observations. We also discuss avenues for future dedicated experiments, which aim at further testing collapse models and the validity of quantum mechanics.

Quantum mechanics radically changed our understanding of Nature. The superposition principle allows for the preparation of quantum systems in coherent superpositions of distinguishable physical configurations. This challenges our classical intuition according to which objects can only be in a one definite physical state at a time. After almost one hundred years of experimental endeavours, the validity of the superposition principle at the microscopic scale is beyond questioning. It has led to an unprecedented understanding of the behaviour of matter and light and to the development of several quantum technologies, such as the laser and the transistor, which are now part of our everyday life.

Despite such success, we face a puzzling situation at the macroscopic scale: we do not experience quantum superpositions, although quantum mechanics does not set any explicit upper bound to the size that such superpositions can have. One possible explanation for the lack of observation of macroscopic quantum superpositions is that the superposition principle progressively breaks down when moving from the microscopic to the macroscopic world¹⁻⁴.

In this regard, spontaneous wavefunction collapse models — or simply collapse models — provide a consistent phenomenological framework for the breakdown of quantum superpositions. The collapse mechanism becomes stronger with the size and complexity of a given system, so that, while the microscopic world is quantum mechanical, the macroscopic world is classical. The collapse dynamics, which is controlled by few parameters, differs from the standard quantum dynamics. The differences can be verified experimentally, and we have recently witnessed an increasing effort in placing

strong experimental bounds on the value of their parameters.

There are essentially two methods to test collapse models. The most direct approach is to perform interferometric experiments, aiming at detecting quantum superpositions (or the lack thereof) with larger and larger objects⁵. The alternative approach is to conduct non-interferometric experiments, where the possible violation of the superposition principle is tested indirectly through various side-effects of the collapse dynamics.

Despite their immediacy, interferometric experiments become significantly harder to perform when the size of the system to test grows. Non-interferometric experiments are relatively easier as they do not require one to prepare the system in a quantum superposition. Instead, they require the precise monitoring of quantities such as the position or the energy.

This review addresses non-interferometric experiments and their ability to provide bounds in the parameter space of two of the most important collapse models, the Continuous Spontaneous Localization model^{6,7} (CSL) and the Diósi-Penrose (DP) one^{1,8}.

1 Theoretical framework of collapse models

Collapse models provide a mathematically and physically consistent dynamical framework, where quantum superpositions and wavepacket reduction are combined. This is achieved by embedding in the Schrödinger equation the mechanism responsible for wavepacket reduction — the not-better-specified collapse of the wavefunction to a definite state upon a measure-

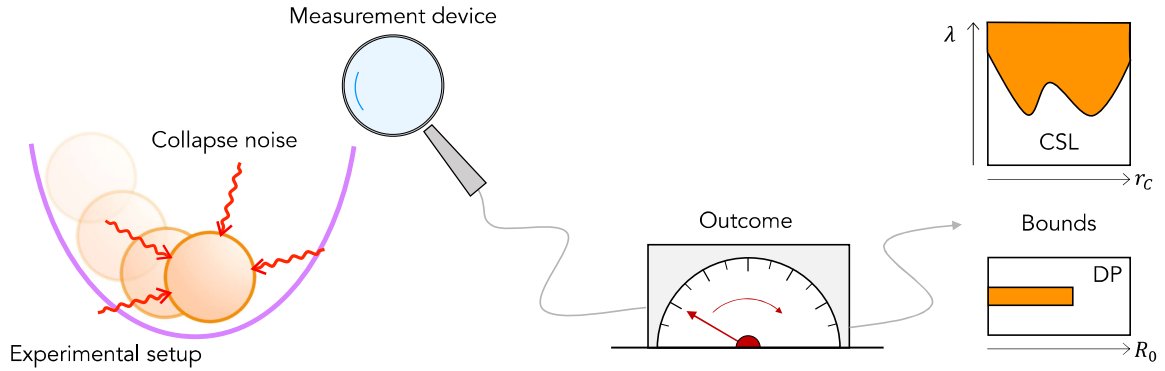


Figure 1. Testing collapse effects using a typical non-interferometric setup. The system (shown as an orange sphere) evolves as described by its quantum mechanical dynamics (for example, there can be a potential, represented by the purple line). The collapse noise (here identified by the red arrows) will modify such dynamics, thus providing predictions which are different from those of quantum mechanics. A suitable measurement device (sketched as a magnifying glass) aims at detecting such a difference. The measurement outcomes are then used to draw the experimental upper bounds on the CSL model and lower bounds on the DP model, which are shown in Fig. 2 and Fig. 3 respectively.

ment according to the standard formulation of quantum theory. Such a mechanism has two features, the first is nonlinearity, which is needed to break the superposition principle. The second one is stochasticity, which allows to recover quantum indeterminacy.

In order to avoid superluminal signaling, non-linear and stochastic terms must be blended carefully^{2,9}. This yields a well specific structure of the dynamical equation. For the models considered in this review, and using the Itô formalism for stochastic differential equations¹⁰, such a dynamical equation reads^{7,11,12}

$$d|\psi_t\rangle = \left[-\frac{i}{\hbar} \hat{H} dt + \int d^3 \mathbf{x} (\hat{M}(\mathbf{x}) - \langle \hat{M}(\mathbf{x}) \rangle_t) dW_t(\mathbf{x}) - \frac{1}{2} \int d^3 \mathbf{x} d^3 \mathbf{y} \mathcal{D}(\mathbf{x} - \mathbf{y}) \prod_{\mathbf{q}=\mathbf{x},\mathbf{y}} (\hat{M}(\mathbf{q}) - \langle \hat{M}(\mathbf{q}) \rangle_t) dt \right] |\psi_t\rangle, \quad (1)$$

where \hbar is the reduced Planck constant. The first term on the right-hand side is the standard quantum contribution as encoded by the system Hamiltonian \hat{H} . The second and third terms describe the stochastic non-linear collapse process weighted by the mass density operator $\hat{M}(\mathbf{x})$, which ensures that the wavefunction is progressively localized in space. The collapse process is driven by the Brownian noise $W_t(\mathbf{x})$ with spatial correlation equal to $\mathcal{D}(\mathbf{x} - \mathbf{y})$, and by the non-linear contribution to the dynamics $\langle \hat{M}(\mathbf{q}) \rangle = \langle \psi_t | \hat{M}(\mathbf{q}) | \psi_t \rangle$.

It is worth stressing that Eq. (1) is built in a way that the statistical operator $\hat{\rho}_t = \mathbb{E}[|\psi_t\rangle \langle \psi_t|]$ (where \mathbb{E} is the stochastic average with respect to the noise) obeys the Lindblad equation

$$\frac{d}{dt} \hat{\rho}_t = -\frac{i}{\hbar} [\hat{H}, \hat{\rho}_t] + \int d^3 \mathbf{x} d^3 \mathbf{y} \mathcal{D}(\mathbf{x} - \mathbf{y}) [\hat{M}(\mathbf{x}), [\hat{M}(\mathbf{y}), \hat{\rho}_t]]. \quad (2)$$

In contrast to the collapse-modified Schrödinger equation, the dynamics in Eq. (2) are linear. This forbids the possibility of superluminal signaling, in spite of the fact that collapse is a non-local process⁹. Although the collapse of the wavefunction is now hidden, Eq. (2) is easier to solve when computing the evolution of expectation values of operators.

Notice that the dynamics resulting from Eq. (1), although not unitary, are norm-preserving and also embed an amplification mechanism: the collapse rate of an object scales roughly with its size. Consequently, one can set extremely small values for the collapse rate for microscopic systems, thus effectively recovering the standard unitary quantum evolution. In turn, the amplification mechanism implies a large collapse rate for macroscopic systems, which remain well localized in space, thus retrieving classical mechanics. In particular, when a microscopic system interacts with a macroscopic measuring device, the collapse dynamics makes sure that the outcomes at the end of the measurement are definite, which are distributed according to the Born rule. In this framework, the Born rule is not assumed but derived¹².

The two most studied collapse models are the CSL and the DP model, which are both described by Eq. (1) with different choices of the correlator $\mathcal{D}(\mathbf{x} - \mathbf{y})$. The CSL model assumes a Gaussian correlator $\mathcal{D}_{\text{CSL}}(\mathbf{x} - \mathbf{y}) = \frac{\lambda}{m_0^2} \exp(-|\mathbf{x} - \mathbf{y}|^2 / 4r_c^2)$ (m_0 is the mass of a nucleon), characterized by two phenomenological parameters: the collapse rate λ , which sets the strength of the collapse for a single nucleon, and the length r_c beyond which spatial superpositions are suppressed. The value proposed by Ghirardi, Rimini, and Weber¹³ (GRW) for the collapse rate is $\lambda = 10^{-16} \text{ s}^{-1}$, which guarantees an effective collapse only for macroscopic systems, whereas Adler¹⁴ proposed the larger values $\lambda = 4 \times 10^{-8 \pm 2} \text{ s}^{-1}$ at $r_c = 10^{-7} \text{ m}$, or alternatively $\lambda = 10^{-6 \pm 2} \text{ s}^{-1}$ at $r_c = 10^{-6} \text{ m}$, under the requirement of a collapse taking place in the mesoscopic regime during the process of latent image formation in photography. On the other hand, there is a broad consensus in setting r_c

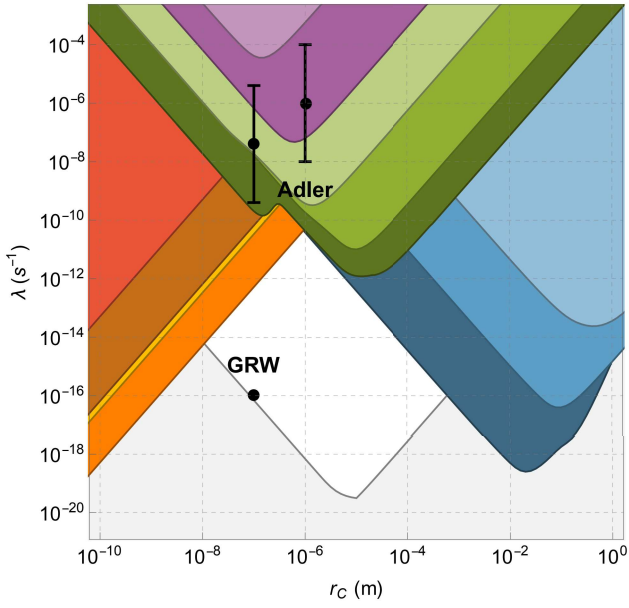


Figure 2. Exclusion plot for the CSL parameters λ and r_c from non-interferometric tests. The colored areas correspond to experimentally excluded regions. The green-colored regions are from cantilever-based experiments with masses of ~ 10 ng³⁸ (light green), ~ 100 ng³⁹ (green), and multilayer structures⁴⁰ (dark green). Blue areas are obtained from gravitational wave detectors^{46–48}: AURIGA (light blue), LIGO (blue) and LISA Pathfinder (dark blue). Purple areas are from optomechanical systems levitating in a linear Paul trap⁴⁹ and a magnetic trap⁵⁰. The orange area is from spontaneous X-ray emission tests⁵¹. The yellow area is from phonon excitation in the CUORE experiment^{27,30}. The brown area is from the heating rate of Neptune⁶³. The red area is drawn from cold-atom experiments³². The theoretical values proposed by GRW¹³ and the ranges proposed by Adler¹⁴ are shown respectively as a black dot and black dots with bars that indicate the estimated range. Finally, the light grey area is excluded not from experiments but from the requirement that macroscopic superpositions do not persist in time, which is the main motivation behind collapse models. Specifically, the (relatively arbitrary but reasonable) requirement adopted here is that a graphene disk of radius $10 \mu\text{m}$, approximately the smallest visible size for a human eye, collapses in 0.01 s, which is about the time resolution of the human eye⁹⁵. The white area is yet to be explored.

within the mesoscopic length scale of $r_c = 10^{-7}$ m. This choice would guarantee microscopic superpositions to survive and the suppression of macroscopic ones, although only experiments can determine its value.

The DP model relates the collapse mechanism to gravity by choosing a correlator proportional to the Newtonian potential $\mathcal{D}_{\text{DP}}(\mathbf{x} - \mathbf{y}) = \frac{G}{\hbar} \frac{1}{|\mathbf{x} - \mathbf{y}|}$, where G is the gravitational constant. When applying the model to a distribution of point-like particles the collapse rate diverges, meaning that the collapse is instantaneous also for microscopic systems. This is clearly falsified by experimental evidence. For this reason, a regularization through the introduction of a spatial cutoff R_0 is needed, which gives a finite size to otherwise point particles.

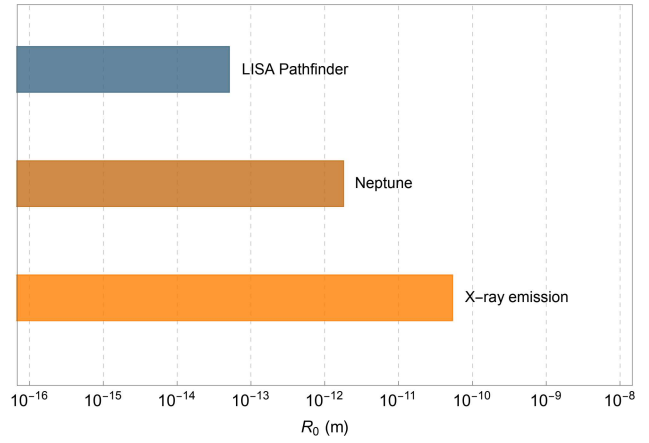


Figure 3. Exclusion plot for the DP parameter R_0 from non-interferometric tests. The colored areas correspond to experimentally excluded values of R_0 . The blue bound is from LISA Pathfinder⁴⁷, the brown area is from the heating rate of Neptune⁶³, the orange one is from X-ray emission tests⁵².

In the first formulation of the model, Diósi⁸ suggested to set R_0 equal to the proton radius of around 10^{-15} m, giving the model the particular appeal of being free from fitting parameters and leading to a collapse time for a proton in a spatial superposition of around 10^6 years, which is fully compatible with observations. However, as we will discuss in detail below, the spontaneous collapses induce an increase of the mean energy of the system, resulting in a heating. Comparison with experimental data shows that $R_0 = 10^{-15}$ m and smaller values must be excluded as they would lead to an unphysical heating¹⁵: the energy increase for a free nucleon would be of the order of 10^{-20} erg/s for $R_0 = 10^{-15}$ m, corresponding to a temperature increase of 7×10^{-5} K/s. Over the life of the Universe, a free nucleon would have developed a temperature of about 3×10^{13} K due to the DP noise, which is not compatible with observations¹⁵. A different estimate for R_0 was given by Penrose^{16,17}, effectively equating R_0 to the width of the wavefunction of the system. This keeps the model free from any fitting parameter endowing it with a cutoff that explicitly depends on the system under scrutiny. Following the most recent literature, we consider R_0 as a free parameter, whose value is eventually constrained by experiments.

The collapse parameters are ultimately bounded by experiments. In what follows, we will review a number of them. For the CSL model, such bounds constrain the maximum value that can be taken by λ at given values of r_c as — according to Eq. (2) — the collapse effect grows with the value of λ . Conversely, for the DP model, lower bounds on R_0 are sought, as the collapse strength depends inversely on this parameter.

Besides collapsing the system's wavefunction (or keeping it localized through time), the noise induced by the collapse mechanism also results in Brownian motion in addition to the system's dynamics. Detecting this motion is the goal of non-interferometric experiments.

2 Interferometric and non-interferometric experiments

The most direct approach for testing collapse models is to prepare a spatial quantum superposition, let the different components interfere — ideally in a noise-free environment — and then measure the corresponding interference pattern⁵. If interference fringes appear, the superposition principle holds for that type of systems within the measurement error, otherwise it is violated. This can be due to different reasons, such as the localisation of the system's wavefunction predicted by a collapse model.

Interferometric experiments face difficulties that limit their capability to place experimental bounds on the collapse parameters. In particular, preparing and maintaining spatial superpositions of massive systems over time is challenging from a technical perspective as it requires isolation from any external agent that might spoil the superposition. Such an external action would prevent the occurrence of possible collapse mechanisms or disguise them. Typically, this requires low temperature, high vacuum, low-vibration conditions. Another major challenge is the experimental preparation of an initial coherent superposition state that is large enough to generate a visible interference pattern. The challenge of the preparation stage grows with the size and mass of the particles at hand. This process should be robust and reproducible as a large number of particles would need to be prepared in nearly identical initial states to allow for the acquisition of sufficient statistics to resolve an interference pattern.

State-of-art interferometric experiments now employ particles of around 10^4 atomic mass units (amu) and have set an upper bound of $\lambda < 10^{-7} \text{ s}^{-1}$ at $r_c = 10^{-7} \text{ m}$ for the CSL model¹⁸. This is a few orders of magnitude away from testing Adler's value and is a billion times weaker than what is needed to probe the GRW value. Probing such a value would need masses of 10^7 amu and a size of the quantum superposition of around 180 nm, maintained for about 20 s. The request on time is too demanding to make such an experiment practical. A potential way forward is to perform experiments on-board of a dedicated satellite to exploit the advantages provided by the space environment^{19,20} as its microgravity environment enables long free-fall times. To date, interferometric experiments have not set relevant bounds for the DP model. However, there are proposals for implementing experiments that need challenging technical developments, mainly concerning how to generate spatial superpositions of massive systems^{21–24}.

As non-interferometric experiments do not rely upon the preparation of quantum superpositions, they provide an important advantage²⁵. In fact, the collapse noise $W_t(\mathbf{x})$ would act on the nucleons of a system regardless of the quantum or classical nature of the state it has been prepared into, making their dynamics stochastic. The nucleons will randomly accelerate, which leads to a variety of effects that will be discussed below. Among them, a violation of the energy conservation principle is predicted. This should not be seen as disturbing

in light of the phenomenological nature of the models being addressed.

As the typical strength of the collapse rate is very small, a successful experiment will still have to suppress other noise sources from the environment, as for the interferometric approach. The non-interferometric strategy is then to monitor the motion of a system in a controlled environment, looking for Brownian fluctuations, whose detection would be a first hint of a collapse effect. The lack of observation of such hints provides a bound on the collapse parameters, and allows one to draw so-called exclusion plots that identify the regions of parameters that need to be explored to rule out a given collapse model. Figs. 2 and 3 report the exclusion plots for the CSL and the DP model, respectively. Below we discuss individually the constraints obtained from the application of non-interferometric strategies.

2.1 Phonons in low temperature experiments

The collapse noise affects the collective dynamics of atoms, and modifies the phonon distribution in bulk materials, leading to an increase of the internal energy of the system^{26,27}. The CSL model predicts a heating power given by

$$P_{\text{CSL}} = \frac{3}{4} \frac{\hbar^2 \lambda m}{m_0^2 r_c^2}, \quad (3)$$

where m is the mass of the system. The system needs to be isolated in order to derive significant bounds. The main step in this direction is to perform the experiment at low temperatures, as in the case of the CUORE experiment²⁸, where crystals of tellurium oxide weighting 340 g are cooled to around 10 mK. Also shielding the setup from other background noises — such as γ radiation or cosmic rays — by resorting to underground facilities can improve the level of isolation²⁹. Nevertheless, dissipative processes due the interaction with the surrounding environment will still take place. Therefore, materials with high density, which will enhance the collapse effect, and low thermal conductivity to reduce dissipation are the best candidates to test collapse-induced heating. Low-temperature experiments³⁰ can reach heating rates as low as $P/m \sim 100 \text{ pW/kg}$. The most accurate modelling of energy deposition from radioactive decays and penetrating muons still leaves a residual heating of around $P/m \sim 10 \text{ pW/kg}$ unaccounted. This in turn sets the bound²⁷ $\lambda < 3.3 \times 10^{-11} \text{ s}^{-1}$ at $r_c = 10^{-7} \text{ m}$ for the CSL model.

2.2 Cold atoms

State-of-the-art experiments in cold-atom technology allow cooling a cloud of atoms down to the pK scale, thus enabling a high degree of control of such systems. The low operating temperature makes these systems good candidates to test the effects of collapse models, although the amplification mechanism can not be exploited due to the negligible interaction among the atoms in the cloud.

As for the system discussed in Sec. 2.1, the collapse noise produces an increase of the energy (temperature) of the atoms

in the cloud at a rate given in Eq. (3), with m now being the mass of an atom. Comparison with experimental data³¹, taking into account several effects including heating induced by three-body interactions or cooling resulting from evaporation, leads to the upper bound $\lambda < 10^{-7\pm 1} \text{ s}^{-1}$ at $r_c = 10^{-7} \text{ m}$. A stronger bound can be obtained by considering diffusion in position³². CSL predicts that the position variance grows as

$$\langle \hat{x}^2 \rangle_t = \langle \hat{x}^2 \rangle_t^{\text{QM}} + \frac{\lambda \hbar^2}{2m_0^2 r_c^2} t^3, \quad (4)$$

where $\langle \hat{x}^2 \rangle_t^{\text{QM}}$ is the standard quantum mechanical spread, while the second term is the CSL-induced contribution. The latter grows as t^3 , contrary to the linear increase of the CSL contribution to the energy. The ideal experiment to test this prediction consists in cooling down an atomic cloud to very low temperatures, and then letting it evolve freely. The CSL model predicts that the collapse noise will make the cloud expand faster than the predictions from quantum mechanics. If such an extra expansion is not observed, this can be used to set bounds on λ and r_c . Application of Eq. (4) to experimental data³³ leads to $\lambda < 5.1 \times 10^{-8} \text{ s}^{-1}$ for the reference value of $r_c = 10^{-7} \text{ m}$.

2.3 Optomechanical systems

Optomechanical systems are based on the interaction between a mechanical oscillator and a radiation field shone on it³⁴. After the system has reached an equilibrium, one can infer the dynamical properties of the mechanical component, and consequently their modification due to external influences such as those caused by collapse, by analyzing the radiation field^{35–37}. The mechanical oscillator, which is driven by the radiation-pressure coupling with the radiation field, is assumed to be immersed in a thermal bath at temperature T , whose action is quantified by a temperature-dependent noise and a dissipation. The overall noisy action on the mechanical system is characterized in terms of the density noise spectrum of the oscillator's position, which reads^{35–37}:

$$S_{\text{DNS}}(\omega) = S_{\text{opto}}(\omega) + \frac{\hbar \omega m \gamma_m \coth(\hbar \omega / 2k_B T) + S_{\text{CM}}}{m^2[(\omega_{\text{eff}}^2 - \omega^2)^2 + \gamma_{\text{eff}}^2 \omega^2]}, \quad (5)$$

where $S_{\text{opto}}(\omega)$ is the standard optomechanical contribution from the radiation field on the mechanical resonator at frequency ω . The second term — the contribution from the environment — is characterized by the mass m of the mechanical part, the mechanical damping γ_m , the effective frequency and damping ω_{eff} and γ_{eff} respectively, where k_B is the Boltzmann constant. Collapse models contribute to the expression of the density noise spectrum with the addition of S_{CM} , which depends on the mass density of the system, is proportional to λ , and can be interpreted as a variation of the equilibrium temperature (or energy E) of the system. Equivalently, due to the equipartition theorem, an increase of the effective energy of the system is translated into an increase of the spread in position^{35–37} given by $\langle \hat{x}^2 \rangle \sim \int d\omega S_{\text{DNS}}(\omega) \propto E + \Delta E_{\text{CM}}$, where ΔE_{CM} is the collapse models' contribution to energy.

Several experiments with optomechanical systems imposed significant bounds on the collapse parameters; we can separate these experiment into three main classes. The first class is that of clamped systems, as cantilevers, where the motion of a ferromagnetic sphere that is attached at the end of a silicon cantilever is examined using a superconducting detector. The system with masses from tens³⁸ to hundreds³⁹ ng is monitored at different temperatures from 10 mK to 1 K to characterize the collapse induced increase of the effective temperature. These tests constrained the CSL model to around $\lambda < 1.9 \times 10^{-8} \text{ s}^{-1}$ at $r_c = 10^{-7} \text{ m}$. Recently, the setup⁴⁰ was specifically tailored for testing the CSL model at $r_c = 10^{-7} \text{ m}$ ⁴¹, yielding an upper bound $\lambda < 2.0 \times 10^{-10} \text{ s}^{-1}$, which completely covers the values suggested by Adler. The second class of experiments includes the gravitational wave detectors LIGO⁴², AURIGA⁴³, and the space-based prototype LISA Pathfinder^{44,45}. These employ macroscopic masses from the kg to the ton scale, whose motion is monitored with optical techniques, making them effectively optomechanical systems. Although being fully in the classical, macroscopic regime, such experiments pose the strongest experimental bounds on the collapse parameters^{46–48} for $r_c > 10^{-5} \text{ m}$. This is due to the fact that for such large masses, the collapse is magnified due to the amplification mechanism. Although the corresponding bounds are the strongest for large values of correlation length r_c , they are softer at $r_c = 10^{-7} \text{ m}$: LIGO⁴² sets $\lambda < 1.0 \times 10^{-5} \text{ s}^{-1}$, AURIGA⁴³ gives $\lambda < 4.6 \times 10^{-2} \text{ s}^{-1}$, while LISA Pathfinder^{44,45} provides $\lambda < 3.8 \times 10^{-9} \text{ s}^{-1}$. The third class of experiments is that of levitated systems. The levitation of spheres of around 0.1 to 5 pg was made possible through the use of a linear Paul trap⁴⁹ and a magneto-levitational trap⁵⁰ at room temperature, respectively. The current bounds obtained from such experiments are comparable to those from interferometric experiments, yielding $\lambda < 4.1 \times 10^{-5} \text{ s}^{-1}$ and $\lambda < 6.7 \times 10^{-7} \text{ s}^{-1}$ for the CSL model at $r_c = 10^{-7} \text{ m}$. Although these bounds are not yet competitive compared to other non-interferometric methods, they hold the promise to provide stricter bounds. One can expect a major improvement when working in cryogenic conditions.

2.4 Gamma and X-ray emission

Brownian motion, such as that induced by the collapse noise, imparts a (random) acceleration to particles, which makes them radiate if charged. As otherwise this radiation would not be there, it can be used to test collapse models.

The most recent analysis applied to the CSL model⁵¹ has shown that the radiation emission rate from a crystal is given by

$$\frac{d\Gamma_{\text{CSL}}}{dE} = N_{\text{atoms}} \frac{(N_A^2 + N_A) \lambda \hbar e^2}{4\pi^2 \epsilon_0 m_0^2 r_c^2 c^3 E}, \quad (6)$$

where N_{atoms} is the total number of atoms, N_A the atomic number, e the elementary charge, ϵ_0 the vacuum's dielectric constant, c the speed of light and E the energy of the emitted photons. Eq. (6) is valid for $E \in [10, 10^5] \text{ keV}$, which corresponds to photon wavelengths larger than the size of a nucleus

but smaller than that of an atom. In this regime, the protons in the same nucleus emit coherently, giving rise the quadratic contribution N_A^2 . Because the electrons emit incoherently from the atomic nuclei, their contribution does not cancel that of the protons and the electrons contribute linearly with N_A . A similar expression is derived for the DP model⁵².

The first application⁵³ of the induced radiation emission rate ruled out the Karolyazy model⁵⁴, which proposes a connection between wavefunction collapse and gravity. It was later applied to the mass-independent version of the CSL model, where the mass density $\hat{M}(\mathbf{x})$ in Eq. (1) is replaced by the particle number density times m_0 , effectively ruling it out⁵⁵.

A recent comparison with data from a dedicated experiment – performed in the underground Gran Sasso laboratories in Italy lead to the strongest bounds on the CSL⁵¹ and on the DP⁵² model of $\lambda < 5.2 \times 10^{-13} \text{ s}^{-1}$ at $r_c = 10^{-7} \text{ m}$ and of $R_0 \geq 0.54 \times 10^{-10} \text{ m}$, respectively. It also ruled out the parameter-free version of the DP model relating R_0 to the width of the wave function, as suggested by Penrose. According to this prescription, one would expect $R_0 \sim 5 \times 10^{-12} \text{ m}$ for Germanium crystal cooled down to 77 K, which is about 10 times smaller than the lower bound set by the experiment.

2.5 Decay of superconducting currents in SQUIDS

Below a critical temperature, metals become superconductors: electrons bind in pairs, so-called Cooper pairs, and flow without resistance on the metal surface⁵⁶. A particularly interesting instance of such devices is given by superconducting quantum interference devices (known as SQUIDS), which are characterized by a superconducting loop interrupted by two Josephson junctions. It was suggested⁵⁷ — and later achieved⁵⁸ — that SQUIDS can be put in the superposition of two macroscopically distinct current states, and that these could be exploited to test the validity of the superposition principle.

Collapse models predict that superconducting currents are unstable, because the collapses tend to localize single electrons, thus breaking Cooper pairs, leading to the decay of the current^{59,60}. Such an effect is suppressed by the small value of the electron mass with respect to the nucleon reference mass, but is enhanced by the large number of electrons taking part in the process. For the CSL model, the decay rate can be approximated as⁶⁰

$$\gamma_{\text{CSL}} = \frac{3}{2\sqrt{\pi}} \frac{N \lambda}{k_F r_c}, \quad (7)$$

where N is the number of Cooper pairs, and k_F is the Fermi momentum. This is compared with the experimental rate^{56,61} $\gamma \sim 3 \times 10^{-13} \text{ s}^{-1}$, which is obtained by measuring the decay of the field produced by the superconducting currents⁶¹, which allows to set an upper bound on the CSL rate of¹⁴ $\lambda < 10^{-3} \text{ s}^{-1}$ at $r_c = 10^{-7} \text{ m}$. The theoretical estimate of the supercurrent decay, however, neglects the recombination of electrons into Cooper pairs, thus the bound could be weaker.

However, because the experimental data on superconducting currents decay are dated⁶¹, more recent measurements could possibly allow to set stronger bounds.

2.6 Astronomical and cosmological observations

Astronomy and cosmology are becoming more and more important for testing collapse models, because they provide an arena, where the collapse effects can build up over very long times and for very large systems¹⁴. In the non-relativistic regime, one can exploit the collapse-induced Brownian motion to set bounds on the collapse parameters, which are reported in Table 1.

The collapse noise reduces the stability of bound systems, and this can be applied to a variety of situations. The dissociation of cosmic hydrogen during the evolution of the Universe¹¹, results in the bound $\lambda < 1 \text{ s}^{-1}$ for $r_c = 10^{-7} \text{ m}$. The same noise, by accelerating protons, perturbs the thermal history of the Universe. Besides the high energy photons considered in Section 2.4, protons will also emit low energy photons, which contribute to the Cosmic Microwave Background (CMB) radiation; precision measurements of the latter give¹⁴ $\lambda < 10^{-5} \text{ s}^{-1}$ for $r_c = 10^{-7} \text{ m}$. Because the emission is not thermal, these photons will distort the spectrum of the CMB. Data from the COBE/FIRAS (Cosmic Background Explorer/Far Infrared Absolute Spectrophotometer) observations bounds the CSL parameters to⁶² $\lambda < 10^{-1} \text{ s}^{-1}$ for $r_c = 10^{-7} \text{ m}$.

The intergalactic medium, consisting of highly ionized hydrogen, is heated by various astrophysical sources and is cooled by adiabatic expansion of the Universe and by recombination cooling of the plasma. As the collapse noise will add to the heating mechanism, it will increase the equilibrium temperature. Observations set the bound¹⁴ $\lambda < 10^{-8} \text{ s}^{-1}$.

Another equilibrium argument can be applied to astronomical and astrophysical bodies, such as Neptune⁶³ and the neutron star⁶⁴ PSR J 1840-1419, which is the coldest neutron star found so far. Under the assumption that the collapse-induced heating is equilibrated by the energy loss due to the radiation emission, as described by the Stefan-Boltzmann law, one obtains $\lambda < 9.4 \times 10^{-7} \text{ s}^{-1}$ for PSR J 1840-1419 and $\lambda < 6.6 \times 10^{-11} \text{ s}^{-1}$ for Neptune.

Collapse models have also been applied to cosmology . They were proposed as candidates to implement an effective cosmological constant⁶⁵, or to justify the emergence of the cosmic structures in the Universe⁶⁶⁻⁶⁸, whose imprint can be found in the observed temperature anisotropies of the CMB. The latter is a remarkable prediction of inflationary cosmology, where theory and observations match very well. Collapse dynamics having acted since shortly after the Big Bang will impact the spectrum of primordial perturbations, both at the scalar and at the tensorial level⁶⁹⁻⁷³.

Under this perspective, observational data applied to cosmic inflation were used to rule out the CSL model for a specific choice of the relativistic collapse operator⁷⁴, but soon after it was shown that a different choice⁷⁵ restores compatibility

Effect	Bound on λ [s ⁻¹]
Non-dissociation of hydrogen ¹¹	< 1
CMB distortion (COBE/FIRAS) ⁶²	$< 10^{-1}$
Protons heating's contribution to the CMB ¹⁴	$< 10^{-5}$
Heating in neutron stars ⁶⁴	$< 9.4 \times 10^{-7}$
Heating of the Intergalactic Medium ¹⁴	$< 10^{-8}$
Heating of Neptune ⁶³	$< 6.6 \times 10^{-11}$

Table 1. Astronomical and cosmological bounds on the CSL model. The listed bounds, which are discussed in Section 2.6, are computed for the reference value of the characteristic length $r_c = 10^{-7}$ m. The strongest bound is reported also in Fig. 2.

of CSL with cosmological observations. The problem is that it is not clear which form collapse models should take in relativistic situations⁷⁶ — and even less in situations where gravitational effects are strong.

3 Perspectives

To further progress in testing collapse models, new dedicated experiments will have to be designed and performed to achieve unprecedented levels of control over the relevant degrees of freedoms of the probe mass. They will push for technological developments, which in turn will open the possibility of discovering new physical properties. Here, we will review some promising avenues that are currently being explored.

The first possibility is to test collapse models using parametric heating of a trapped nanosphere. Specifically, a Paul trap is proposed⁷⁷ to measure the heating rate of a single-charged levitated nanosphere. The hybrid trap cools the mechanical motion to a low temperature, and afterwards the optical field of the cavity is turned off to let the nanosphere evolve freely before measuring the particle's energy. By comparing the predictions with a model including the heating induced by the collapse mechanism one can test the parameter range to $\lambda = 10^{-12}$ s⁻¹ for a background pressure of 10^{-13} mbar and a temperature of the mechanical system of 20 K.

Although being commonly the first candidate in many experiments, translational degrees of freedom are not the only available option. Indeed, it is possible to provide very stringent constraints on the collapse parameters by using roto-vibrational degrees of freedom. A master equation describing the roto-vibrational diffusion due to collapse effects has been derived⁷⁸, which is used in a non-interferometric proposal⁴⁸ applied to an optomechanical system. Such proposal demonstrated that roto-vibrational diffusion can be employed to restrict the uncharted values of the collapse parameters using both lab-based and space-bound configurations, potentially down to the GRW parameters.

Performing non-interferometric experiments in free-fall is another possible way to enhance the constraints on the collapse parameters¹⁹. Indeed, in free fall, the system does not require external potentials that would inevitably introduce extra noises in the system's dynamics, hindering those due to the collapse mechanism. Concrete possibilities on ground are provided by the Bremen drop-tower⁷⁹ or the Hannover

Elevator platform⁸⁰. Such experiments could also be performed in dedicated space missions^{19,81} or on board the International Space Station, where other quantum experiments were already conducted⁸².

The performance of collapse models test can also be enhanced significantly by incorporating information-theoretic techniques of sensing and metrology⁸³. In particular, building on the success in estimating the temperature of open quantum systems^{84,85}, quantum parameter estimation techniques can be employed as a way to infer the equilibrium temperature of a mechanical oscillator potentially subjected to the effects of the CSL model.

One can complement the latter schemes with the use of hypothesis testing methods. By making use of Bayesian test protocols applied to both matter-wave interferometry^{86,87} and non-interferometric settings⁸⁸, one can address the hypothetical modifications of quantum theory induced by the occurrence of collapse mechanisms.

Current state-of-art non-interferometric investigations can be extended to the possible generalizations of collapse models. The CSL and DP models resort to a white noise, which is not physical, which moreover breaks the energy conservation of the system. The full resolution of both limitations requires the development of an underlying theory, which is not yet available, although some work in this direction has been made². Meanwhile, non-white and dissipative generalizations of the CSL^{89,90} and DP⁹¹ models have been formulated. In the former extension, a cut-off frequency Ω_0 , a new collapse parameter, characterizes the noise spectrum, making it more similar to other physical noises. On the other hand, the dissipative extension avoids the energy of an otherwise isolated system to diverge. In such a model, the system eventually thermalizes to a temperature T_0 , which is a further collapse parameter. There are currently several experiments providing bounds on the collapse parameters of these extensions^{49,92-94}. However, with the additional parameters Ω_0 and T_0 , the parameter space widens, and thus it becomes more challenging to fully cover its unexplored regions.

More ambitiously, collapse models call for an underlying deeper-level theory where the unitary dynamics, as well as the collapse, emerge naturally. This would explain the physical origin of the collapse of the wave function, be it related to gravity as suggested by Penrose¹ and others — or to yet unidentified degrees of freedom².

The interest in collapse models and their experimental testing has grown considerably in the last decade, which is also sustained by significant technological developments. The unprobed part of the parameter space has been greatly reduced, pushing the limits of quantum theory further. Nevertheless, the question on whether quantum mechanics is valid universally up to the macroscopic scale remains open. And only experiments can tell.

Acknowledgments

The authors acknowledge fruitful discussions with Roger Penrose and Andrea Vinante on various aspects of the models and the related experiments. MC and MP are supported by UK EPSRC (Grant No. EP/T028106/1). SD and AB acknowledge financial support from INFN. LF, MP, HU and AB acknowledge financial support from the H2020 FET Project TEQ (Grant No. 766900). MP acknowledges the DfE-SFI Investigator Programme (Grant No. 15/IA/2864), the Leverhulme Trust Research Project Grant UltraQute (Grant No. RGP-2018-266), the Royal Society Wolfson Research Fellowship scheme (Grant No. RSWFR3\183013) and International Mobility Programme. HU acknowledges financial support from the Leverhulme Trust (Grant No. RPG-2016-04), and EPSRC (Grant No. EP/V000624/1). AB acknowledges the Foundational Questions Institute and Fetzer Franklin Fund, a donor advised fund of Silicon Valley Community Foundation (Grant No. FQXi-RFP-CPW-2002) and the University of Trieste.

Competing interests

The authors declare no competing financial/non-financial interests.

References

1. Penrose, R. On gravity's role in quantum state reduction. *Gen. relativity gravitation* **28**, 581–600 (1996).
2. Adler, S. *Quantum Theory as an Emergent Phenomenon* (Cambridge University Press, Cambridge, 2004).
3. Leggett, A. J. The quantum measurement problem. *Science* **307**, 871–872 (2005).
4. Weinberg, S. The trouble with quantum mechanics. *The New York Rev. Books*, January 19 (2017).
5. Arndt, M. & Hornberger, K. Testing the limits of quantum mechanical superpositions. *Nat. Phys.* **10**, 271–277 (2014).
6. Pearle, P. Combining stochastic dynamical state-vector reduction with spontaneous localization. *Phys. Rev. A* **39**, 2277–2289 (1989).
7. Ghirardi, G. C., Pearle, P. & Rimini, A. Markov processes in hilbert space and continuous spontaneous localization of systems of identical particles. *Phys. Rev. A* **42**, 78–89 (1990).
8. Diosi, L. A universal master equation for the gravitational violation of quantum mechanics. *Phys. Lett. A* **120**, 377–381 (1987).
9. Gisin, N. Stochastic quantum dynamics and relativity. *Helvetica Phys. Acta* **63**, 363–371 (1989).
10. Arnold, L. *Stochastic Differential Equations* (John Wiley & Sons, New York, 1971).
11. Pearle, P. & Squires, E. Bound state excitation, nucleon decay experiments and models of wave function collapse. *Phys. Rev. Lett.* **73**, 1–5 (1994).
12. Bassi, A., Lochan, K., Satin, S., Singh, T. P. & Ulbricht, H. Models of wave-function collapse, underlying theories, and experimental tests. *Rev. Mod. Phys.* **85**, 471–527 (2013).
13. Ghirardi, G. C., Rimini, A. & Weber, T. Unified dynamics for microscopic and macroscopic systems. *Phys. Rev. D* **34**, 470–491 (1986).
14. Adler, S. L. Lower and upper bounds on CSL parameters from latent image formation and IGM heating. *J. Phys. A* **40**, 2935–2957 (2007).
15. Ghirardi, G., Grassi, R. & Rimini, A. Continuous-spontaneous-reduction model involving gravity. *Phys. Rev. A* **42**, 1057–1064 (1990).
16. Penrose, R. Wavefunction collapse as a real gravitational effect. In *Mathematical physics 2000*, 266–282 (World Scientific, London, 2000).
17. Penrose, R. On the gravitization of quantum mechanics 1: Quantum state reduction. *Foundations Phys.* **44**, 557–575 (2014).
18. Fein, Y. Y. et al. Quantum superposition of molecules beyond 25 kDa. *Nat. Phys.* **15**, 1242–1245 (2019).
19. Gasbarri, G. et al. Testing the foundation of quantum physics in space via interferometric and non-interferometric experiments with mesoscopic nanoparticles. *Commun. Phys.* **4**, 155 (2021).
20. Belenchia, A. et al. Test quantum mechanics in space—invest us \$1 billion. *Nature* **596**, 32–34 (2021).
21. Marshall, W., Simon, C., Penrose, R. & Bouwmeester, D. Towards quantum superpositions of a mirror. *Phys. Rev. Lett.* **91**, 130401 (2003).
22. Machluf, S., Japha, Y. & Folman, R. Coherent Stern–Gerlach momentum splitting on an atom chip. *Nat. Commun.* **4**, 2424 (2013).
23. Bateman, J., Nimmrichter, S., Hornberger, K. & Ulbricht, H. Near-field interferometry of a free-falling nanoparticle from a point-like source. *Nat. Commun.* **5**, 4788 (2014).
24. Howl, R., Penrose, R. & Fuentes, I. Exploring the unification of quantum theory and general relativity with a Bose–Einstein condensate. *New J. Phys.* **21**, 043047 (2019).

25. Collett, B. & Pearle, P. Wavefunction collapse and random walk. *Foundations Phys.* **33**, 1495–1541 (2003).
26. Bahrami, M. Testing collapse models by a thermometer. *Phys. Rev. A* **97**, 052118 (2018).
27. Adler, S. L. & Vinante, A. Bulk heating effects as tests for collapse models. *Phys. Rev. A* **97**, 052119 (2018).
28. Alduino, C. et al. The projected background for the CUORE experiment. *The Eur. Phys. J. C* **77**, 543 (2017).
29. Mishra, R., Vinante, A. & Singh, T. P. Testing spontaneous collapse through bulk heating experiments: An estimate of the background noise. *Phys. Rev. A* **98**, 052121 (2018).
30. Pobell, F. *Matter and methods at low temperatures*, vol. 2 (Springer, Berlin, 2007).
31. Laloë, F., Mullin, W. J. & Pearle, P. Heating of trapped ultracold atoms by collapse dynamics. *Phys. Rev. A* **90**, 052119 (2014).
32. Bilardello, M., Donadi, S., Vinante, A. & Bassi, A. Bounds on collapse models from cold-atom experiments. *Phys. A* **462**, 764–782 (2016).
33. Kovachy, T. et al. Matter wave lensing to picokelvin temperatures. *Phys. Rev. Lett.* **114**, 143004 (2015).
34. Aspelmeyer, M., Kippenberg, T. J. & Marquardt, F. Cavity optomechanics. *Rev. Mod. Phys.* **86**, 1391–1452 (2014).
35. Bahrami, M., Paternostro, M., Bassi, A. & Ulbricht, H. Proposal for a noninterferometric test of collapse models in optomechanical systems. *Phys. Rev. Lett.* **112**, 210404 (2014).
36. Nimmrichter, S., Hornberger, K. & Hammerer, K. Optomechanical sensing of spontaneous wave-function collapse. *Phys. Rev. Lett.* **113**, 020405 (2014).
37. Diósi, L. Testing spontaneous wave-function collapse models on classical mechanical oscillators. *Phys. Rev. Lett.* **114**, 050403 (2015).
38. Vinante, A. et al. Upper bounds on spontaneous wave-function collapse models using millikelvin-cooled nanocantilevers. *Phys. Rev. Lett.* **116**, 090402 (2016).
39. Vinante, A., Mezzena, R., Falferi, P., Carlesso, M. & Bassi, A. Improved noninterferometric test of collapse models using ultracold cantilevers. *Phys. Rev. Lett.* **119**, 110401 (2017).
40. Vinante, A. et al. Narrowing the parameter space of collapse models with ultracold layered force sensors. *Phys. Rev. Lett.* **125**, 100404 (2020).
41. Ferialdi, L. & Bassi, A. Continuous spontaneous localization reduction rate for rigid bodies. *Phys. Rev. A* **102**, 042213 (2020).
42. Abbott, B. P. et al. Observation of gravitational waves from a binary black hole merger. *Phys. Rev. Lett.* **116**, 061102 (2016).
43. Vinante, A., AURIGA Collaboration et al. Present performance and future upgrades of the auriga capacitive readout. *Class. Quantum Gravity* **23**, S103–S110 (2006).
44. Armano, M. et al. Sub-femto-g free fall for space-based gravitational wave observatories: LISA pathfinder results. *Phys. Rev. Lett.* **116**, 231101 (2016).
45. Armano, M. et al. Beyond the required LISA free-fall performance: new LISA Pathfinder results down to 20 μ Hz. *Phys. Rev. Lett.* **120**, 061101 (2018).
46. Carlesso, M., Bassi, A., Falferi, P. & Vinante, A. Experimental bounds on collapse models from gravitational wave detectors. *Phys. Rev. D* **94**, 124036 (2016).
47. Helou, B., Slagmolen, B., McClelland, D. E. & Chen, Y. LISA pathfinder appreciably constrains collapse models. *Phys. Rev. D* **95**, 084054 (2017).
48. Carlesso, M., Paternostro, M., Ulbricht, H., Vinante, A. & Bassi, A. Non-interferometric test of the continuous spontaneous localization model based on rotational optomechanics. *New J. Phys.* **20**, 083022 (2018).
49. Pontin, A., Bullier, N., Toroš, M. & Barker, P. Ultranarrow-linewidth levitated nano-oscillator for testing dissipative wave-function collapse. *Phys. Rev. Res.* **2**, 023349 (2020).
50. Zheng, D. et al. Room temperature test of the continuous spontaneous localization model using a levitated micro-oscillator. *Phys. Rev. Res.* **2**, 013057 (2020).
51. Donadi, S. et al. Novel CSL bounds from the noise-induced radiation emission from atoms. *The Eur. Phys. J. C* **81**, 773 (2021).
52. Donadi, S. et al. Underground test of gravity-related wave function collapse. *Nat. Phys.* **17**, 74–78 (2021).
53. Diósi, L. & Lukács, B. Calculation of X-ray signals from Károlyházy hazy space-time. *Phys. Lett. A* **181**, 366–368 (1993).
54. Karolyhazy, F. Gravitation and quantum mechanics of macroscopic objects. *Il Nuovo Cimento A* **42**, 390–402 (1966).
55. Fu, Q. Spontaneous radiation of free electrons in a non-relativistic collapse model. *Phys. Rev. A* **56**, 1806–1811 (1997).
56. Tinkham, M. *Introduction to Superconductivity* (McGraw Hill, New York, 1996).
57. Leggett, A. J. Macroscopic quantum systems and the quantum theory of measurement. *Prog. Theor. Phys. Suppl.* **69**, 80–100 (1980).
58. Friedman, J. R., Patel, V., Chen, W., Tolpygo, S. K. & Lukens, J. E. Quantum superposition of distinct macroscopic states. *Nature* **406**, 43–46 (2000).
59. Rae, A. I. M. Can GRW theory be tested by experiments on SQUIDS? *J. Phys. A* **23**, L57–L60 (1989).

60. Buffa, M., Nicosini, O. & Rimini, A. Dissipation and reduction effects of spontaneous localization on superconducting states. *Foundations Phys. Lett.* **8**, 105–125 (1995).
61. Crowe, J. W. Trapped-flux superconducting memory. *IBM J. Res. Dev.* **1**, 294–303 (1957).
62. Lochan, K., Das, S. & Bassi, A. Constraining continuous spontaneous localization strength parameter λ from standard cosmology and spectral distortions of cosmic microwave background radiation. *Phys. Rev. D* **86**, 065016 (2012).
63. Adler, S. L., Bassi, A., Carlesso, M. & Vinante, A. Testing continuous spontaneous localization with Fermi liquids. *Phys. Rev. D* **99**, 103001 (2019).
64. Tilloy, A. & Stace, T. M. Neutron star heating constraints on wave-function collapse models. *Phys. Rev. Lett.* **123**, 080402 (2019).
65. Josset, T., Perez, A. & Sudarsky, D. Dark energy from violation of energy conservation. *Phys. Rev. Lett.* **118**, 021102 (2017).
66. Perez, A., Sahlmann, H. & Sudarsky, D. On the quantum origin of the seeds of cosmic structure. *Class. Quantum Gravity* **23**, 2317–2354 (2006).
67. Landau, S. J., Scóccola, C. G. & Sudarsky, D. Cosmological constraints on nonstandard inflationary quantum collapse models. *Phys. Rev. D* **85**, 123001 (2012).
68. Das, S., Lochan, K., Sahu, S. & Singh, T. P. Quantum to classical transition of inflationary perturbations: Continuous spontaneous localization as a possible mechanism. *Phys. Rev. D* **88**, 085020 (2013).
69. Cañate, P., Pearle, P. & Sudarsky, D. Continuous spontaneous localization wave function collapse model as a mechanism for the emergence of cosmological asymmetries in inflation. *Phys. Rev. D* **87**, 104024 (2013).
70. Das, S., Sahu, S., Banerjee, S. & Singh, T. P. Classicalization of inflationary perturbations by collapse models in light of BICEP2. *Phys. Rev. D* **90**, 043503 (2014).
71. León, G., Landau, S. J. & Piccirilli, M. P. Inflation including collapse of the wave function: the quasi-de Sitter case. *The Eur. Phys. J. C* **75**, 393 (2015).
72. Banerjee, S., Das, S., Kumar, K. S. & Singh, T. P. Signatures of spontaneous collapse-dynamics-modified single-field inflation. *Phys. Rev. D* **95**, 103518 (2017).
73. León, G. & Piccirilli, M. P. Generation of inflationary perturbations in the continuous spontaneous localization model: The second order power spectrum. *Phys. Rev. D* **102**, 043515 (2020).
74. Martin, J. & Vennin, V. Cosmic microwave background constraints cast a shadow on continuous spontaneous localization models. *Phys. Rev. Lett.* **124**, 080402 (2020).
75. Gundhi, A., Gaona-Reyes, J. L., Carlesso, M. & Bassi, A. Impact of dynamical collapse models on inflationary cosmology. *Phys. Rev. Lett.* **127**, 091302 (2021).
76. Bengochea, G. R., León, G., Pearle, P. & Sudarsky, D. Discussions about the landscape of possibilities for treatments of cosmic inflation involving continuous spontaneous localization models. *The Eur. Phys. J. C* **80**, 1021 (2020).
77. Goldwater, D., Paternostro, M. & Barker, P. Testing wave-function-collapse models using parametric heating of a trapped nanosphere. *Phys. Rev. A* **94**, 010104 (2016).
78. Schrirski, B., Stickler, B. A. & Hornberger, K. Collapse-induced orientational localization of rigid rotors. *J. Opt. Soc. Am. B* **34**, C1–C7 (2017).
79. Gierse, A. et al. A fast and self-acting release-caging-mechanism for actively driven drop tower systems. *Microgravity Sci. Technol.* **29**, 403–414 (2017).
80. Lotz, C. et al. Tests of additive manufacturing and other processes under space gravity conditions in the Einstein-Elevator. *Logist. Journal: Proc.* **2020** (2020).
81. Kaltenbaek, R. et al. Macroscopic quantum resonators (MAQRO): 2015 update. *EPJ Quantum Technol.* **3**, 5 (2016).
82. Elliott, E. R., Krutzik, M. C., Williams, J. R., Thompson, R. J. & Aveline, D. C. NASA's Cold Atom Lab (CAL): system development and ground test status. *npj Microgravity* **4**, 16 (2018).
83. Paris, M. G. A. Quantum estimation for quantum technology. *Int. J. Quantum Technol.* **7**, 125–137 (2009).
84. Brunelli, M., Olivares, S. & Paris, M. G. A. Qubit thermometry for micromechanical resonators. *Phys. Rev. A* **84**, 032105 (2011).
85. Brunelli, M., Olivares, S., Paternostro, M. & Paris, M. G. A. Qubit-assisted thermometry of a quantum harmonic oscillator. *Phys. Rev. A* **86**, 012125 (2012).
86. Schrirski, B., Nimmrichter, S. & Hornberger, K. Quantum-classical hypothesis tests in macroscopic matter-wave interferometry. *Phys. Rev. Res.* **2**, 033034 (2020).
87. Schrirski, B., Hornberger, K. & Nimmrichter, S. How to rule out collapse models with BEC interferometry. *arXiv eprint 2008.13580* (2020).
88. Marchese, M. M., Belenchia, A., Pirandola, S. & Paternostro, M. An optomechanical platform for quantum hypothesis testing for collapse models. *New J. Phys.* **23**, 043022 (2021).
89. Adler, S. L. & Bassi, A. Collapse models with non-white noises. *J. Phys. A* **40**, 15083 (2007).
90. Smirne, A. & Bassi, A. Dissipative continuous spontaneous localization (CSL) model. *Sci. Reports* **5**, 12518 (2015).

91. Bahrami, M., Smirne, A. & Bassi, A. Role of gravity in the collapse of a wave function: A probe into the Diósi-Penrose model. Phys. Rev. A **90**, 062105 (2014).
92. Nobakht, J., Carlesso, M., Donadi, S., Paternostro, M. & Bassi, A. Unitary unraveling for the dissipative continuous spontaneous localization model: Application to optomechanical experiments. Phys. Rev. A **98**, 042109 (2018).
93. Carlesso, M., Ferialdi, L. & Bassi, A. Colored collapse models from the non-interferometric perspective. The Eur. Phys. J. D **72**, 159 (2018).
94. Vinante, A., Gasbarri, G., Timberlake, C., Toroš, M. & Ulbricht, H. Testing dissipative collapse models with a levitated micromagnet. Phys. Rev. Res. **2**, 043229 (2020).
95. Toroš, M., Gasbarri, G. & Bassi, A. Colored and dissipative continuous spontaneous localization model and bounds from matter-wave interferometry. Phys. Lett. A **381**, 3921–3927 (2017).